Comptes Rendus

Géoscience

Sciences de la Planète

Hervé Guillon, Jean-Louis Mugnier, Arthur Schwing
and Jean-François Buoncristiani

Glacial drainage development controls temporal and spatial fluctuations of sediment flux in Mont Blanc's North face

Original Article — Geomorphology

Glacial drainage development controls temporal and spatial fluctuations of sediment flux in Mont Blanc's North face

Hervé Guillon [*, a], **Jean-Louis Mugnier** [a], **Arthur Schwing** [a] and **Jean-François Buoncristiani** [b]

[a] Institut des Sciences de la Terre, Université Grenoble Alpes/Université Savoie Mont-Blanc/CNRS, CS40700, 38058 Grenoble Cedex 9, France

[b] Biogéosciences, UMR 6282 CNRS / Université Bourgogne Franche-Comté, Dijon, France

E-mails: herve@guillon.xyz (H. Guillon), jean-louis.mugnier@univ-smb.fr (J.-L. Mugnier), schwing_tur@hotmail.fr (A. Schwing), jfbuon@u-bourgogne.fr (J.-F. Buoncristiani)

Abstract. Present-day global warming raises important issues regarding sediment flux from glaciated catchments. The detrital export from such environments results from erosion processes operating in three geomorphic domains: the supraglacial rockwalls, the ice-covered substratum and the proglacial area, downstream from the glacier. The dominant process controlling present-day sediment export from glaciated catchments remains debated with most studies underlining the paraglacial dynamics in the glacier forefront. This study nuances these observations by quantifying the contribution from each geomorphic domain to the export of a glaciated catchment in the North face of Mont-Blanc (France). High resolution hydro-sedimentary flux data were acquired during eight years in two proglacial streams with contrasting glacio-hydrological characteristics, Bossons and Crosette streams. In the Bossons stream catchment, the sediment response highlights the initiation of the dendritic drainage network beneath the glacier, the short-lived evacuation of an annual storage during the early melt-season and its subsequent steadier regime. In addition, three years exhibit late melt season exports which are uncorrelated with temperature or rainfall. The evolution of the drainage network throughout the melt season explains the evacuation of the annual and pluri-annual subglacial sediment stocks. In addition, glacial retreat in link with higher melt rate allows for exporting a pluri-annual sediment stock stored beneath the glacier. To conclude, the present-day sediment response in Bossons catchment displays distinct components with characteristic timescales and is dampened by intermediate storage controlled by drainage development and extreme events in the glacial and proglacial domains.

Keywords. Glacial erosion, Subglacial processes, Subglacial drainage, Hydro-sedimentary, Sediment response.

Manuscript received 8 March 2022, revised 14 June 2022, accepted 16 June 2022.

* Corresponding author.

1. Introduction

Ice volume and glaciated surface area have drastically reduced [Vincent et al., 2017] during the 20th century, and projections indicate further decline during the 21st century [Zekollari et al., 2018]. Observed and projected change to the headwaters of mountain watersheds leads to complex perturbations of their hydrologic regime [Mackay et al., 2019] and downstream ecosystems [Canadell et al., 2019]. In that context, water and sediment flux in glaciated watersheds will display significant change. Sediment export from glaciated catchments is pivotal: it is likely to increase [Delaney and Adhikari, 2020], modulates flood risk and reservoir sedimentation [Ehrbar et al., 2018], impacts river management [O'Briain, 2019], and possibly inputs large amount of sediment to downstream systems.

Sediment export from glaciated catchments is best described by the paraglacial concept: a source-to-sink approach linking sediment export to climatic conditions inducing varying ice-coverage [Ballantyne, 2002b]. Formally, "paraglacial" refers to processes and landforms conditioned by the antecedent presence of a glacier [Church and Ryder, 1972, Ballantyne, 2002a,b]. Conceptually, sediment is produced during cool, dry glaciation periods and exported during warmer, wetter inter-glacial periods. For example, the paraglacial response to the last glacial maximum led to a significant increase in sediment discharge in the Alps [Kellerer-Pirklbauer et al., 2010, Ravazzi et al., 2012], in British Columbia [Church and Ryder, 1972, Kovanen and Slaymaker, 2015], in the Cascade Range [Moon et al., 2015] and in the Teton Range [Larsen et al., 2016]. Similarly, there is ample evidence of ongoing paraglacial adjustment linked to more recent glacial retreat [Knight and Harrison, 2014, 2018] with examples from Svalbard [Bourriquen et al., 2018], Iceland [Staines et al., 2014], the French Alps [Kirkbride and Deline, 2018], the Swiss Alps [Curry et al., 2006, Eichel et al., 2018], the Austrian Alps [Savi et al., 2014, Avian et al., 2018], the Himalayas [Owen and Sharma, 1998, Morin et al., 2018], Alaska [Klaar et al., 2014], and British Columbia [Leggat et al., 2015].

Importantly, the sediment signal from a glaciated catchment integrates processes of transport and production over three distinct geomorphic domains: (i) the supraglacial rockwalls, (ii) the ice-covered subglacial substratum, and (iii) the glacier forefront. Each of these geomorphic domains is defined by its position relative to the glacier and exhibits distinct geomorphic processes. Historically, discharge and sediment concentration measured at a distance downstream from glaciers served as a proxy to assess glacial erosion response [Baëff, 1891, Boissier, 1916, Rothlisberger and Lang, 1987] as well as interactions between subglacial hydrology and sediment dynamics [Anderson et al., 2003, Riihimaki, 2005]. In recent years, hydro-sedimentary records have increased in resolution [Guillon et al., 2018] and duration [Rainato et al., 2016, Morin et al., 2018], with longer duration records often accounting for sediment processes both beneath the glacier and in its vicinity [Micheletti et al., 2015, Lane et al., 2017]. However, since measuring erosion processes occurring beneath ice or at the active front of a glacier is difficult, the links between the sediment signal and subglacial processes remain largely unexplored from observational data [Jaeger and Koppes, 2016].

In this study, to characterize sediment transfer and to document possible links with subglacial processes, we developed a data-driven heuristic approach based on data acquired in the Mont-Blanc Massif in the Bossons glacier catchment. This analysis adds to the growing body of literature documenting sediment activity in the forefront of retreating Alpine glaciers while unplanned observations provide field-based insights on the processes occurring beneath this glacier. In addition, we offer a counterpoint to most existing observations by quantifying the sediment export from three distinct geomorphic domains. The core data of this study is an eight-year hydro-sedimentary record [Guillon et al., 2015a] which has not been accomplished in its entirety till date.

2. Study area and available datasets

The focus of this study is the iconic Bossons glacier flowing on the North face of Mont-Blanc from its summit (4810 m asl) to ~1450 m asl (Figure 1). Such an elevation range leads to varied thermal conditions at the base of the glacier with the transition between areas of the glacier with cold and temperate basal ice occurring at ~3300 m asl [Le Meur and Vincent, 2006]. Above this Limit of Cold Ice (LCI), the
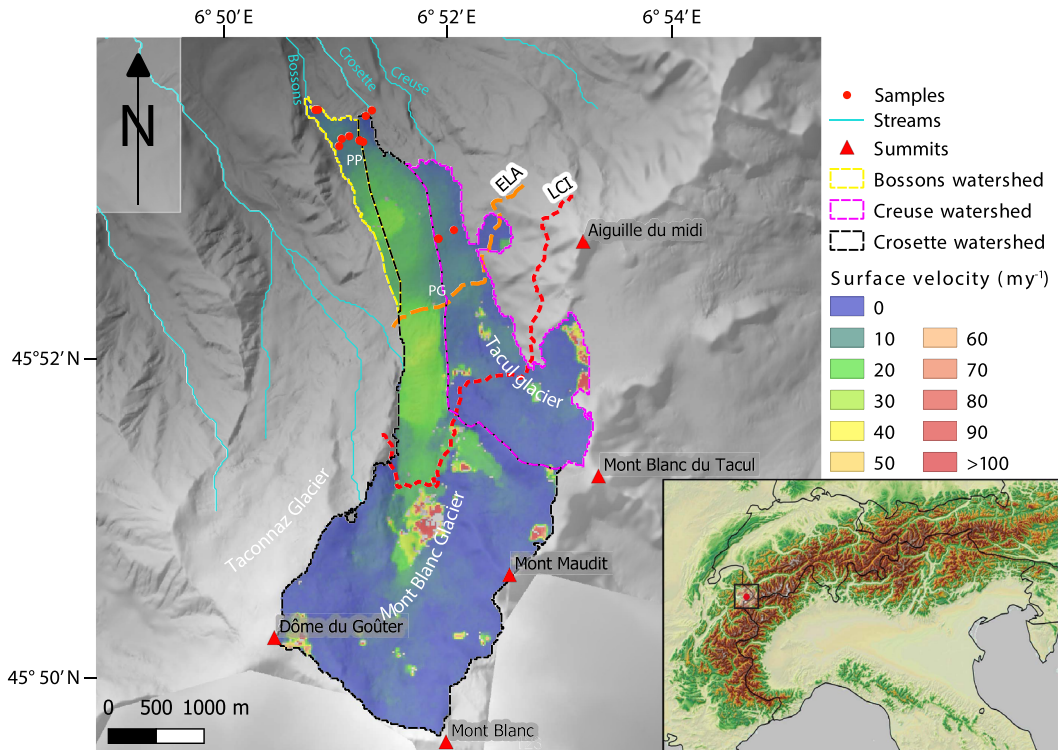
Figure 1. Map of the northward flowing Bossons Glacier in the North Face of Mont-Blanc. The Equilibrium Line Altitude (ELA), Limit of Cold Ice (LCI) and limits of subglacial watershed assessed by Godon et al. [2013] are reported. Surface ice velocities were derived for the year 2005 [Berthier et al., 2005].

basal ice is far from its melting point [Vincent et al., 2007] and erosion is proved to be negligible [Godon et al., 2013]. The limit between the ablation and accumulation area of the Bossons glacier, or Equilibrium Line Altitude (ELA), is ~2750 m asl [Godon et al., 2013].

The glacial drainage system beneath the Bossons glacier has three main outlets: the Creuse stream, the Crosette stream, and the Bossons stream (Figure 1). The Creuse stream drains the Tacul glacier, a glacial tributary to the Bossons glacier, and its high elevation and difficult field conditions make it impossible to be reliably monitored. The Crosette stream drains most of the Bossons glacier up to Mont-Blanc summit, and its catchment includes both cold and temperate basal conditions. The Bossons stream drains the lowermost part of the Bossons glacier and its catchment lies both below the ELA and LCI (Figure 1).

Slope, surface velocity, and thickness vary along the long profile of the Bossons glacier. The Bossons glacier exhibits a steep average slope of ~27°, and its surface is rugged and hummocky with sérac falls with slopes greater than 45°. The ablation area presents two flatter zones: Plan Glacier (PG) and Plateau des Pyramides (PP), at 2600 and 1800 m asl, respectively [Figure 1, Magnin et al., 2020]. Surface velocity and ice thickness were estimated for the Bossons glacier from a mass-balance and flow modeling approach [Huss and Farinotti, 2012], and surface velocities were also derived from satellite imagery [Berthier et al., 2005, Fallourd et al., 2011]. Both estimates highlight that steeper and thinner areas flow faster than the flatter, thicker sections of Plan Glacier and Plateau des Pyramides (Figure 1).

Efforts to assess sediment origin and transport processes have been carried out in the Bossons glacier catchment since 2004 (Table 1), providing

Table 1. Melt season and monitoring durations for each year

Station	Year	Melt season duration (days)	Monitoring duration during the melt season (days)	Melt season monitored (%)	Total monitoring* duration (days)	Year monitored (%)
Bossons	2009	n/a	52	28	52	14
	2010	n/a	75	40	75	21
	2011	197	78	40	96	26
	2012	183	93	51	148	41
	2013	157	71	45	109	30
	2014	205	136	66	136	37
	2015	212	117	55	137	38
	2016	171	142	83	171	47
Crosette	2013	157	74	47	98	27
	2014	171	105	61	191	52
	2016	85	85	100	170	47

*This represents the total duration of data used for flux calculation; the length of the recorded discharge is longer and allows for identification of melt season initiation.

insights regarding the origin and transport of sediment in its glacial and proglacial domains. In the glacial domain, variations in the proportion of the supraglacial load transferred to the Crosette and Bossons streams were identified using lithological analysis [Godon et al., 2013] and cosmogenic nuclides content [Guillon et al., 2015b]. Cosmogenic nuclides result from interactions between minerals and cosmic rays and their concentration has two end-members: a negligibly-concentrated substratum shielded by ice and a highly-concentrated supraglacial load derived from exposed rockwalls. A mixture model between those two end-members estimated the fraction C of the sediment discharge from the glacier corresponding to supraglacial inputs [Guillon et al., 2015b]. This methodology was updated by Sarr et al. [2019] who demonstrated that the concentration of cosmogenic nuclides in supraglacial load is both independent from clast size and represents the long term erosion of the rockwalls when numerous (several tens or even hundreds) clasts are amalgamated in the measured sample.

In the proglacial domain, the analysis of digital elevation models and of the position of ~1000 radio-frequency-tagged particles over three years indicated a decennial transit time for coarse particles [Guillon et al., 2015c, Guillon, 2016]. In addition, direct sampling of bedload under various flow conditions suggested that bedload is a minor component of the sediment flux [Godon et al., 2014]. Because of such a slow and limited export of coarse particles, the remainder of this study is limited to suspended sediment; the bedload component is likely to be contained within the uncertainty of the values presented. Analysis of suspended load measurements acquired in multiple points of the glacial catchment highlighted that the glacier is the dominant source of suspended sediment during the melt season [Guillon et al., 2018]. Furthermore, the proglacial alluvial plain acts as a buffer, storing sediments until the transport capacity allows for exporting either during high discharge events linked to precipitation or when the sediment concentration from the glacier drops at the end of the melt season [Guillon et al., 2018]. Datasets collected in the Bossons glacier catchment were made publicly available [Godon et al., 2014, Guillon et al., 2015a,c], and this study is the first to make use of the entire eight-year hydro-sedimentary record. Finally, the glacial retreat was evaluated by the National Observation Service GLACIOCLIM (SNO/INSU) hosted at the Observatoire des Sciences de l'Univers de Grenoble.
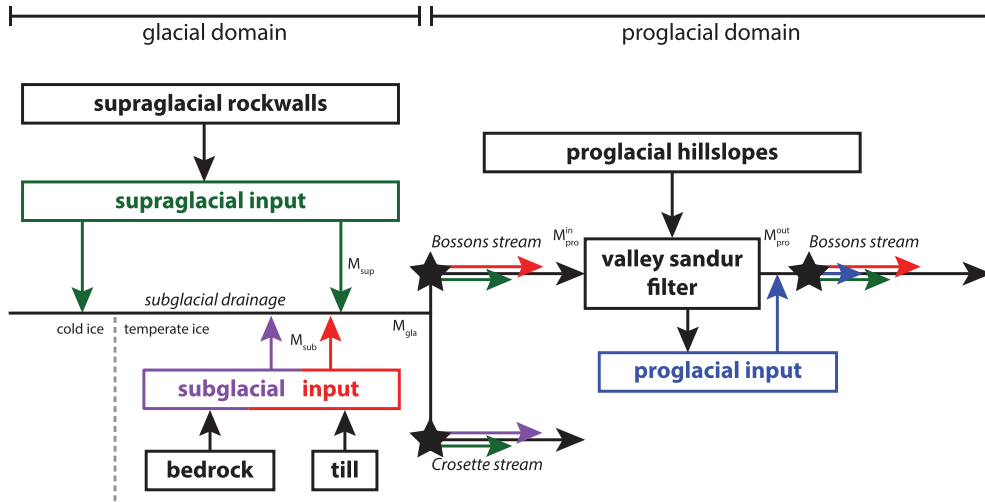
Figure 2. Data framework in Bossons glacier catchment. Stars represent sampling locations.

Table 2. Parameter values

Parameter	Description	Value
M_{gla}	Combined input from supraglacial and subglacial domains	-
M_{sup}	Input from the supraglacial domain	-
M_{sub}	Input from the subglacial domain	-
M_{pro}	Input from the proglacial domain	-
M_{pro}^{in}	Mass entering the proglacial buffer	-
M_{pro}^{out}	Mass exiting the proglacial buffer	-
τ	Meltseason duration	-
R	Rainfall	-
C(Bossons)	Supraglacial to subglacial input ratio of Bossons stream (-)	0.089 ± 0.025
C(Crosette)	Supraglacial to subglacial input ratio of Crosette stream (-)	0.018 ± 0.0075
p	Supraglacial load proportion exiting at Bossons (-)	0.83 ± 0.34

All hydro-sedimentary parameters obtained from Guillon et al. [2015a].

3. Estimating sediment input by geomorphic domains with a data-driven heuristic approach

A data-driven heuristic approach translated findings from previous research into an actionable model to estimate the annual sediment input from the supraglacial, subglacial and proglacial domains (Figure 2, Table 2). This three-step approach estimated: (i) the combined input from the supraglacial and subglacial domains, M_{gla}; (ii) the distinct inputs from the supraglacial and subglacial domains, M_{sup} and M_{sub}, respectively; and (iii) the sediment input of the proglacial domain, M_{pro}. Sediment input has unit of mass and was derived by integrating the sediment flux (discharge × concentration) with respect to time.

First, during the time period corresponding to the melt season τ, the input from the entire glacial system $M_{gla} = M_{sup} + M_{sub}$ was expressed as a function of rainfall R and mass entering and exiting the proglacial alluvial buffer, M_{pro}^{in} and M_{pro}^{out}, respectively:

$$M_{gla}(\tau, R \geq 0) = \overbrace{M_{pro}^{in}(\tau, R = 0)}^{\text{dry periods}} + \overbrace{M_{pro}^{in}(\tau, R > 0)}^{\text{wet periods}}. \quad (1)$$

Since, at the annual timescale, during dry periods, the sediment mass originating from the glacier is equivalent to the mass exiting the alluvial area [Guillon et al., 2018]:

$$M_{\text{gla}}(\tau, R \geq 0) \simeq M_{\text{pro}}^{\text{out}}(\tau, R = 0) + M_{\text{pro}}^{\text{in}}(\tau, R > 0). \quad (2)$$

The mass of sediment entering the proglacial system during rain events was approximated using a simple statistical model leveraging data acquired simultaneously upstream and downstream of the alluvial area (See Appendix A).

Second, updating the mixing model from Guillon et al. [2015b] with additional measurements from Sarr et al. [2019], the respective input from supraglacial and subglacial domains (Table B1) was estimated from the fraction C of the glacial sediment discharge corresponding to supraglacial inputs:

$$M_{\text{sup}} = C \cdot M_{\text{gla}} \quad (3)$$

$$M_{\text{sub}} = (1 - C) \cdot M_{\text{gla}}. \quad (4)$$

The total mass coming from the supraglacial rockwalls is the sum of the contribution in each catchment:

$$M_{\text{sup}}(\text{total}) = M_{\text{sup}}(\text{Bossons}) + M_{\text{sup}}(\text{Crosette}). \quad (5)$$

In the absence of Crosette data, the total supraglacial input was estimated from the proportion of supraglacial load exiting in the Bossons stream catchment where the hydro-sedimentary record is longer (Table 1):

$$p = \frac{C(\text{Bossons})}{C(\text{Bossons}) + C(\text{Crosette})} \quad (6)$$

$$M_{\text{sup}}(\text{total}) = \frac{M_{\text{sup}}(\text{Bossons})}{p}. \quad (7)$$

Third, the sediment input from the proglacial area M_{pro} was expressed as the sediment export during wet periods of the melt season and outside of the melt season.

$$M_{\text{pro}} = \underbrace{M_{\text{pro}}^{\text{out}}(\tau, R > 0) - M_{\text{pro}}^{\text{in}}(\tau, R > 0)}_{\text{proglacial export during melt season precipitations}}$$
$$+ \underbrace{M_{\text{pro}}^{\text{out}}(\neg\tau, R \geq 0)}_{\text{everything outside of melt season}} . \quad (8)$$

Similarly to Guillon et al. [2018], uncertainties were propagated from the initial in-situ hydro-sedimentary measurement to the sediment input using a Monte-Carlo scheme.

The annual sediment input from the supraglacial, subglacial and proglacial domains was augmented by

analyzing cumulative export and glacial front position. As the glacier is the dominant source of sediment during periods without precipitation [Guillon et al., 2018], analyzing the cumulative sediment export estimates the sediment response from the glacial domain. Finally, to estimate the impact of glacial retreat on sediment flux, subglacial sediment export was correlated with the glacial retreat.

4. Results

In this section, we report the main results of this study: (i) the intensity of the sediment export is different between the three geomorphic domains; (ii) export of the subglacial sediment occurs during characteristic periods; and (iii) sediment flux correlates positively with glacial retreat.

Our data-driven heuristic approach estimated the sediment budget for the Bossons glacier catchment in three distinct geomorphic domains: the supraglacial rockwalls, the ice-covered substratum, and the proglacial area (Figure 3). The intensity of the annual sediment export was derived for each geomorphic domains (Table 3) from the exported sediment mass (Tables C1–C2). For the proglacial domain, high values of the sediment export occurred in 2009 and 2010, and most likely in 2015 and 2016—based on the total export from the catchment. The high 2015–2016 values are directly linked to an observed extreme event affecting the proglacial hillslopes [Guillon et al., 2018]. Such a link is unclear for years 2009 and 2010 which exhibit improbable outliers during rain events. Then, excluding years 2009–2010 and 2015–2016 yields a conservative estimate of the average proglacial sediment flux, $22 \pm 16 \times 10^3$ kg·yr^{-1}. In the subglacial domain drained by the Crosette stream, the 2013–2014 sediment fluxes were higher than 300×10^3 kg·yr^{-1} while the value for 2016 was much lower, $41 \pm 8 \times 10^3$ kg·yr^{-1}. Similarly, in the subglacial domain drained by the Bossons stream, the sediment fluxes were highly variable, ranging from $58 \pm 18 \times 10^3$ kg·yr^{-1} to $266 \pm 47 \times 10^3$ kg·yr^{-1}. Excluding the estimate from 2011 which corresponds to a limited sampling of the melt-season leads to an average value of $194 \pm 48 \times 10^3$ kg·yr^{-1} for the subglacial sediment flux in the Bossons stream catchment. In the supraglacial domain, sediment flux appears relatively low and constant with a mean value of $20 \pm 7 \times 10^3$ kg·yr^{-1}.

Table 3. Sediment flux and average sediment flux by year and by domain

Year	Sediment flux (10^3 kg·yr^{-1})					Meltwater volume (10^6 m^3)	
	Bossons (total)	Bossons (subglacial)	Supraglacial	Bossons (proglacial)	Crosette (subglacial)	Bossons	Crosette
2009	183 ± 29	121 ± 83	12 ± 9	$51 \pm 85^*$	n/a	n/a	n/a
2010	699 ± 109	252 ± 69	24 ± 10	$423 \pm 134^*$	n/a	n/a	n/a
2011	77 ± 20	$58 \pm 18^*$	6 ± 2	13 ± 6	n/a	0.88	n/a
2012	308 ± 52	266 ± 47	26 ± 8	16 ± 13	n/a	1.1	n/a
2013	161 ± 35	122 ± 27	17 ± 6	27 ± 24	302 ± 112	0.98	8.2
2014	231 ± 44	184 ± 35	25 ± 7	29 ± 19	399 ± 105	0.83	3.8
2015	806 ± 112	n/a	n/a	n/a	n/a	1.7	n/a
2016	1311 ± 190	n/a	n/a	n/a	$41 \pm 8^*$	1.2	0.45
Weighted mean	228 ± 42	194 ± 48	20 ± 7	22 ± 16	357 ± 108		

Meltwater volume was derived for years with high resolution data by integrating discharge from mid-June to mid-September.

*This value has been excluded from the mean estimate.

The eight-year-long observation record in the Bossons glacier catchment provides an avenue to understand the variation observed in subglacial sediment fluxes. Such an inter-annual variation (Figure 3) appears to be linked to an intra-annual variation of the sediment export (Figure 4a). Focusing on sediment discharge from the glacier only, we present the cumulative sediment export during the periods without precipitations of the melt-season from 2009 to 2010 and from 2012 to 2014. The change of slope of this cumulative export indicates distinct events. The melt-season usually starts with a limited export until a marked step occurs. For the years 2013–2014, such an initial export is more gradual. Most years, after this initial step, the melt season cumulative export presents a steady slope. Notwithstanding, from late July to September 2012, a drastic change in the slope of the cumulative export indicates the continuous export of a significant amount of sediment from the system. While less prominent than this 2012 late season export, a similar event happened from mid-August to mid-September 2014 and a short-lived export occurred in late August 2010. Interestingly, such events are uncorrelated with a change in discharge (Figure 4b) which weakly predicts sediment export (Figure C1).

Subglacial sediment fluxes in the Bossons stream catchment appears to be correlated with glacial front
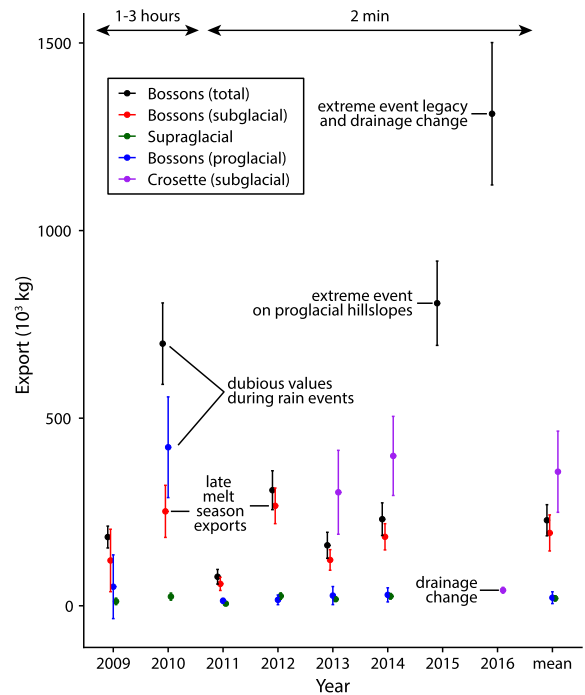

Figure 3. Annual sediment export by geomorphic domain of the Bossons glacier catchment. Weighted average for each geomorphic domain are displayed at the right. Between 2009 and 2010, the data were at best acquired with a hourly time step. Since 2011, data were acquired with a 2-min time step.
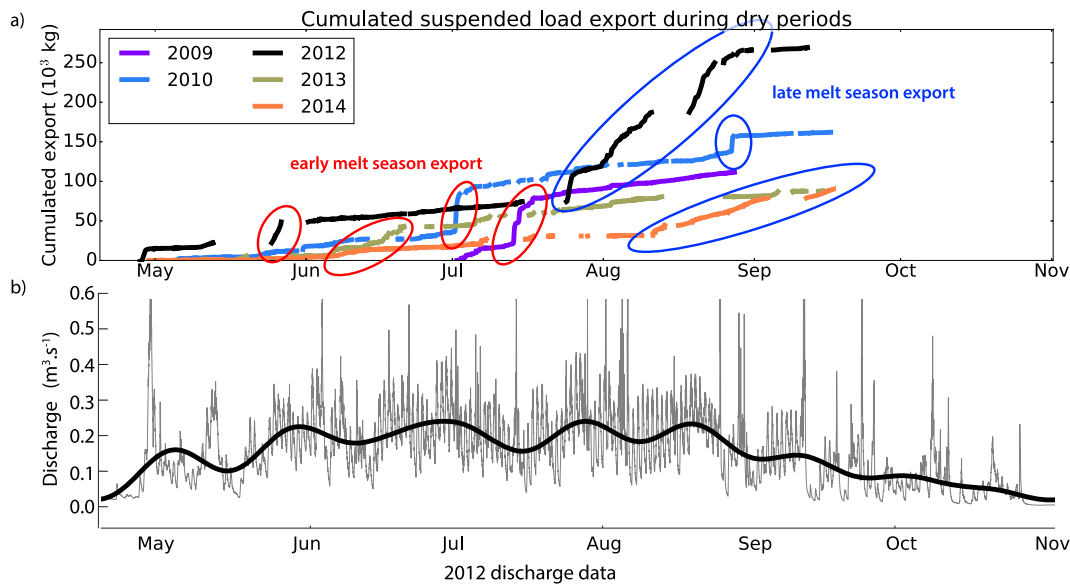
Figure 4. (a) Cumulative export during dry periods of suspended load for Bossons stream for 2009, 2010, 2012, 2013 and 2014. (b) Discharge during year 2012. Note the lack of increased discharge when sediment export increases in August 2012.
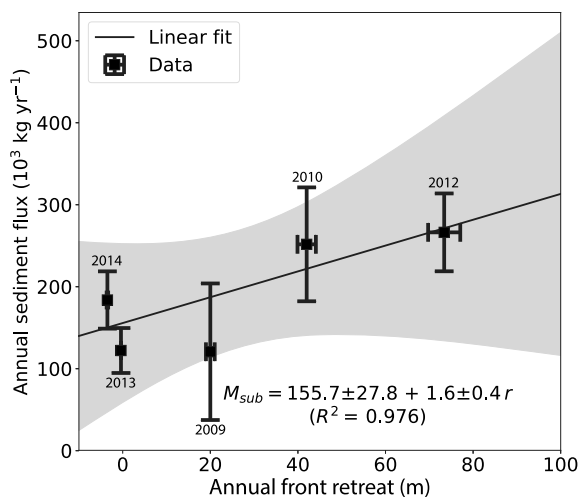

Figure 5. Relation between subglacial sediment flux and glacial front retreat. The amount of Bossons glacier's retreat was evaluated by GlacioClim at the Observatoire des Sciences de l'Univers de Grenoble. The 95% confidence interval is represented by the gray area.

retreat (Figure 5). Glacial front retreat is here measured positively in the direction of the retreat (i.e. upstream from a reference position). The linear relationship between subglacial sediment flux and the

annual retreat of the glacier is significant ($R^2 = 0.98$, t-test's p-value $\ll 0$). While such a correlation is impacted by the limited number of observations, the form of the linear fit summarizes insights gained from studying the cumulative sediment exports (Figure 4). The linear model expresses the subglacial sediment flux M_{sub} as a function of the retreat r: $M_{sub} = 158 + 1.6\,r$. This relationship suggests, in the absence of glacial front retreat, a base sediment flux of $\sim150 \times 10^3$ kg·yr^{-1}, and implies an increase of the sediment export when the glacial front retreats.

5. Discussion

In this section, we discuss the main implications of our observations: (i) variations in the subglacial drainage development induce spatio-temporal variations in subglacial sediment export; and (ii) the present-day sediment signal in a glaciated catchment is a signal with multiple frequencies and intermittent dampening.

5.1. *Variations in subglacial drainage induce variations in subglacial sediment export*

Previous research has documented and linked seasonal variations in water discharge with the

evolution of the glacial drainage system. The annual cycle of water discharge from a glacier starts with a quiescent winter phase ending with the first major glacial flood [Rothlisberger and Lang, 1987]. This so-called spring event corresponds to the initiation of the melt season which ultimately wanes and reaches a new dormant winter phase. In addition to melt rate, the modulation of the amplitude and frequency of the daily glacial floods is tied to the competition between two types of subglacial drainage: a non-dendritic, disconnected, diffuse network, and a dendritic, connected, channelized network [Fountain and Walder, 1998, Figure 6a,b]. The start of the melt season marks the transition from diffuse to channelized network and progressive fragmentation of the channelized drainage system late in the meltseason participates in decreasing runoff [Rada and Schoof, 2018].

This seasonal evolution of the subglacial drainage system impacts subglacial sediment production and transport. Subglacial sediment production occurs through two main processes: abrasion and quarrying. Abrasion, the sand-paper-like action of the basal ice on its substratum, is mainly dependent on the sliding velocity and subglacial water pressure [Hallet, 1979, 1981]. In particular, basal water pressure induces a partial decoupling from the bed, promoting higher sliding velocities and higher abrasion [e.g., Iken and Bindschadler, 1986, Bartholomaus et al., 2008]. Quarrying is equally controlled by variation in basal water pressure, which progressively weakens and ultimately plucks portions of the substratum [Iverson, 2012]. Such fluctuations in basal water pressure occur daily and at the season scale [Nanni et al., 2020]. For example, during spring, the initiation of the melt season in a still developing drainage system increases meltwater pressure and leads to accelerated sliding and abrasion [Ugelvig et al., 2018]. Increasing meltwater pressure, sliding, or abrasion may also occur later in the melt season, if the drainage system is unable to efficiently accommodate meltwater. Anderson et al. [2003] documented for example a short-lived sliding event linked to a glacial flood. In contrast with abrasion peaking in spring, quarrying correlates with shorter-term transient increases of the deviatoric stress in the bedrock which occur mostly late in the melt season when water pressure reduces in a well-developed drainage system [Ugelvig et al., 2018].

As for production, subglacial sediment transport is linked to the seasonal evolution of the subglacial drainage system. The diffuse drainage system is associated with low sediment export while the channelized drainage system leads to higher sediment export [Swift et al., 2002]. Furthermore, diffuse and channelized systems are end-member descriptions and, more generally, the pressurization of the drainage system impacts its transport capacity [Beaud et al., 2018]. In consequence, the initiation of the melt season is associated with a sediment pulse corresponding to the export of a winter sediment stock [Riihimaki, 2005]. The sediment export then decreases progressively over the course of the melt season [Guillon et al., 2018]. Yet, the development of the channelized drainage may reach subglacial sediment pockets leading to their subsequent evacuation [Anderson et al., 2003].

The hydro-sedimentary response from the Bossons stream exemplifies these seasonal changes in subglacial hydro-sedimentary response. Conforming to early season spring events flushing winter sediment stock, the cumulative sediment export exhibits a marked increase at the start of most melt seasons (Figure 4). In addition, distinct export events occurred also late in the melt season of years 2010, 2012 and 2014. However, the timing and duration of these exports rule out a dependence on short-lived acceleration of the glacier [Anderson et al., 2003] or on increased quarrying [Ugelvig et al., 2018]. In particular, it is unlikely that increased quarrying leads to such a rapid response in terms of suspended sediment exported from the glacial system. Rather, these exports strongly suggest the existence of a pluri-annual sediment stock beneath the Bossons glacier, only accessed some years, and which export is controlled by the development of the subglacial drainage system (Figure 6c).

Comparing the sediment export from the Crosette and Bossons streams underlines a major shift in drainage pattern at the scale of the entire glacial system, re-routing meltwater previously exiting at the Crosette outlet to Bossons outlet (Figures 3, 6d). While the subglacial sediment export from the Crosette stream drastically decreases between years 2013–2014 and year 2016, the Bossons stream total export records its highest value in 2016. This 2016 export compounds inputs from the supraglacial, subglacial, and proglacial domains, and is likely heav-
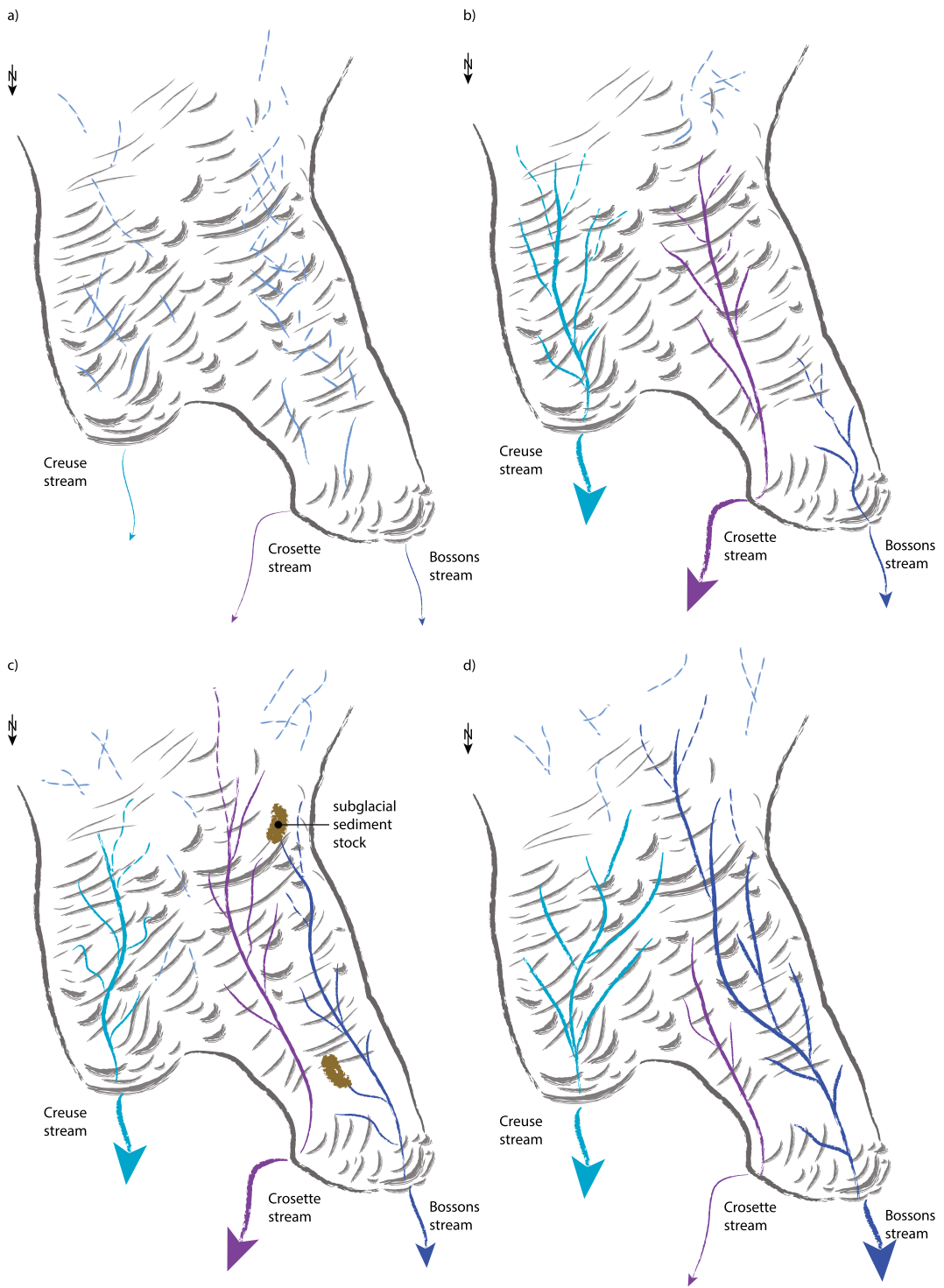
Figure 6. Caption continued on next page.

Figure 6 (cont.). Schematic of different configurations of the subglacial drainage system of Bossons glacier. (a) Diffuse drainage systems in both catchments (e.g. during winter); (b–d) dendritic drainage systems (e.g. during summer and autumn) evolving from one year to the other: (b) well developed in Crosette subglacial catchment, modestly developed in Bossons subglacial catchment; (c) dendritic drainage systems, moderately developed in Crosette subglacial catchment, less developed in Bossons subglacial catchment and reaching subglacial sediment stocks; (d) dendritic drainage systems, minimal in Crosette subglacial catchment, maximal in Bossons subglacial catchment with capture of the upper part of the subglacial drainage catchment.

ily impacted by the legacy of an extreme event that occurred in 2015 on proglacial hillslopes. Nonetheless, the drastic difference in sediment exports of the Crosette and Bossons streams between years 2013–2014 and year 2016 indicates a significant shift in the entire drainage system beneath the Bossons glacier. This is further supported by the observation of increased meltwater volumes for the Bossons stream and decreased meltwater volumes for the Crosette stream over the same time period (Table 3). In addition, the varying total meltwater volume suggests further change in meltwater routing, potentially with temporary storage beneath the glacier as evidenced in the Creuse catchment [Berthet, 2016].

Observations within the Bossons glacier catchment and previous literature suggest causes for the fluctuations in subglacial drainage evidenced from hydro-sedimentary measurements. The subglacial drainage system beneath the Bossons glacier is likely dependent on subglacial topography and melt rate. First, the subglacial topography of the area drained by Bossons stream is probably hummocky considering the steepness of its terminal part as well as the ruggedness of most of its supraglacial topography. Such rugosity is conducive of a stochastic development of the subglacial drainage and of the temporary storage of sediment, especially in the thinner terminal part of the glacier [Beaud et al., 2018]. Furthermore, the terminal part of the Bossons glacier catchment is constituted by the flatter Plateau des Pyramides (PP, Figure 1). The substratum beneath this area is likely over-deepened which may feedback into sediment storage [Magnin et al., 2020]. Second, transfer from meltwater to the base of the glacier has been evidenced on the Bossons glacier [Guillon et al., 2015b] and may stimulate the development of the drainage network. Such a transfer might explain the correlation evidenced between glacial retreat and sediment export (Figure 5). Our observations indi-

cate that an important glacial retreat is the manifestation of high ablation rate that likely invigorates the development of the glacial drainage system, increasing its likelihood to reach subglacial sediment pockets (Figure 6).

5.2. *A synoptic view of the modern day sediment response in a glaciated catchment*

Unexpectedly, the dominant source of the sediment export from the Bossons catchment is the glacial system, and in particular subglacial sediment (Figure 3). This contrasts with numerous studies linking the dominant export of small scale [Leggat et al., 2015, Rainato et al., 2016] and large scale systems [Staines et al., 2014, Hinderer et al., 2013, Morin et al., 2018, Bourriquen et al., 2018] with recently exposed surfaces being impacted by extreme events [Rainato et al., 2016, Morin et al., 2018] while transitioning from gullying to solifluction to stabilisation [Eichel et al., 2018].

Nonetheless, the sediment conveyor belt in the proglacial domain is efficiently jammed by the stability of hillslopes [Micheletti et al., 2015] and by sediment buffers in the alluvial area or on slopes [Lane et al., 2017, Guillon et al., 2018, Kirkbride and Deline, 2018]. These discontinuities highlight both the importance of connectivity in glaciated environments [Cossart and Fressard, 2017, Kirkbride and Deline, 2018] and of the timescale of the paraglacial response. While the dominant source was previously evidenced in the Bossons catchment [Guillon et al., 2018], these authors' data corresponds to only one melt-season. The present study strengthens previous findings by leveraging an eight-year hydro-sedimentary record, and separating the glacial contributions between subglacial and supraglacial sources.

Combining findings from previous research, an eight-year hydro-sedimentary record, and sediment source identification shows that the present-day sediment response in the Bossons catchment has distinct components with characteristic timescales, controls, and intermediate storage. In the lowermost part of the catchment corresponding to the proglacial area, the sediment flux is low compared to the subglacial sediment flux (Figure 3) and appears mainly controlled by the occurrence of extreme events [Guillon et al., 2018]. In addition, at the daily, seasonal and annual scales, the proglacial alluvial area acts as a buffer controlled by the transport capacity of the stream [Guillon et al., 2018]. Within this proglacial fluvial environment, the transit time of the coarse fraction is thought to be ~10 years [Guillon, 2016, Guillon et al., 2015c]. Beneath the Bossons glacier, the evacuation of the subglacial erosion products is mainly determined by the development of the drainage network, flushing out annual and pluri-annual sediment pockets (Figure 6). In the uppermost part of the catchment, rockwalls provide supraglacial debris, a fraction of which is transferred at the bottom of the glacier [Guillon et al., 2015b]. However, the low supraglacial sediment flux we report is indicative of the long-term (millennium scale) erosion of the sidewalls [Sarr et al., 2019] delayed by the multi-decennial supraglacial, englacial and subglacial transport and is unlikely to fully represent modern conditions.

The sediment discharge from the Bossons catchment is a signal with multiple frequencies and intermittent dampening. Regardless of the dominant erosion processes occurring in a catchment—here, subglacial erosion—the first-order control on glaciated sediment export is climate change [Knight and Harrison, 2014]. The general response of landscapes to long-term climatic perturbation has been conceptualized as a signal with multiple frequencies and a degree of dampening describing reactive and buffered landscapes, respectively [Allen, 2005]. In addition, optimal conditions for the frequency of the climate forcing maximize erosion amplitude [Godard et al., 2013]. In the Bossons catchment, the present-day climate forcing optimally drives an efficient reaction in terms of subglacial processes while proglacial erosion has already reacted to the perturbation and is now buffered. With the notable exception of Knight and Harrison [2018], this nuanced synoptic view

is missing from conceptualizations of present-day paraglacial response, is likely to help organizing the existing hydro-sedimentary records and solidifies the need for continuous hydro-sedimentary measurements. In particular, the lack of long-term spatially-distributed high-resolution observations of present-day sediment flux limits the ongoing scientific debate regarding the scaling between subglacial erosion processes and glacier dynamics [e.g., Koppes et al., 2015, Cook et al., 2020] relying so far on a mostly disparate combination of data with few notable exceptions [Herman et al., 2015]. Finally, clearly inferring subglacial sediment processes from hydro-sedimentary data, and comparing findings between observational and modelling studies is hindered by known unknowns to be ideally derived concomitantly with sediment fluxes: surface velocities, extent and type of subglacial drainage, and conditions at the ice-substratum interface (thermal regime, hardness, basal stress, debris concentration).

6. Conclusion

The ongoing glacial retreat perturbs the hydrologic regime and ecosystems of Alpine watersheds. In that context, understanding the interactions between glacier flow, meltwater and sediment export from glaciated catchments is critical. In the present study, to document subglacial sediment processes and further the comprehension of the sediment response to climate change, we developed a data-driven heuristic approach of the sediment transfers based on an eight-year hydro-sedimentary record of a glaciated catchment in the Mont-Blanc Massif. Our results highlight that, in the studied catchment and at first order, drainage development controls sediment evacuation. In addition, the main geomorphic domains defined by the proglacial area, the supraglacial rockwalls and the ice-covered substratum exhibit distinct intermediate storage and sediment exports. In that system, the buffered proglacial landscape is a minor component of the total export and reacts weakly to present-day glacial retreat. Conversely, enhanced glacial retreat in link with higher melt rate allows for exporting a pluri-annual sediment stock stored beneath the glacier. These findings nuance previous studies which mainly underlined the dominant role of paraglacial dynamics in the glacier forefront and calls for long-term high-resolution obser-

vations of present-day sediment flux from glaciated catchments. Organizing and analyzing such existing and warranted hydro-sedimentary records will benefit from describing present-day sediment response as a signal with multiple frequencies and intermittent dampening.

Conflicts of interest

The authors declare no competing financial interest.

Dedication

The manuscript was written with contributions from all authors. All authors have given approval to the final version of the manuscript.

Acknowledgments

Appendix A. Monte-Carlo simulation of sediment flux

Observations in the challenging environment of the high Alpine mountains often have data gaps. In a previous study, missing data in Bossons catchment were estimated using multi-linear models combining measurements at three stations [Guillon et al., 2018]: one at Crosette outlet and two in Bossons catchment, upstream and downstream from the proglacial alluvial area. However, the dataset from Crosette stream catchment has a shorter duration than the one acquired in Bossons stream catchment (Table 1), and an alternative method was needed to estimate the

sediment flux entering the proglacial alluvial area. This was needed to estimate the sediment flux during the rain events of the melt season, when a significant portion of the export is contributed by the proglacial domain. However, because of the complexity of the steep, multi-threaded proglacial stream, a simple one-dimensional hydraulic model was unable to produce satisfactory results [Guillon, 2016]. Furthermore, the same discharge impulse has vastly different response in terms of concentration (Figure A1). In the following, as simple process-based modeling fails, we described the dynamics of the alluvial area at the season scale with a simple statistical model.

A simple statistical framework identified a parameter describing the dynamics of the alluvial area at the seasonal scale, then performed statistical modeling with Monte-Carlo simulations. Observations of the proglacial dynamics [Guillon et al., 2018] underlined a dependence between discharge, Q, and the order of magnitude of the ratio of upstream and downstream sediment flux, F_{in} and F_{out} respectively (Figure A2). We define this ratio between the sediment flux entering and exiting the proglacial alluvial area as $\alpha = F_{in}/F_{out}$. If $\alpha < 1$ ($F_{in} < F_{out}$), the proglacial area contributes sediment; if $\alpha > 1$ ($F_{in} > F_{out}$), part of the sediment flux is trapped in the proglacial area. To account for the dependence with discharge and for the order of magnitude, the logarithm of α was normalized by the discharge, Q, defining a discharge independent logarithmic ratio:

$$\beta = \frac{\log_{10}(\alpha)}{Q} = \frac{\log_{10}(F_{in}/F_{out})}{Q}. \qquad (9)$$

To describe the discharge independent logarithmic ratio of sediment flux, β, a maximum likelihood estimate (MLE) estimated the best-fit parameters of an array of statistical distributions. In practice, MLE minimizes the negative log-likelihood, $-\log\mathscr{L}$ to identify the best fist parameters. A Kolmogorov–Smirnov test then provided a distance measure D between candidate and data distributions. This distance was compared to a critical value depending on the number of observations, n, and a significance level, fixed here at 5%. A distribution providing a good fit for the data has a minimal log-likelihood $-\log\mathscr{L}$ and a Kolmogorov–Smirnov test value, $\sqrt{n}D$, minimally lower than the critical
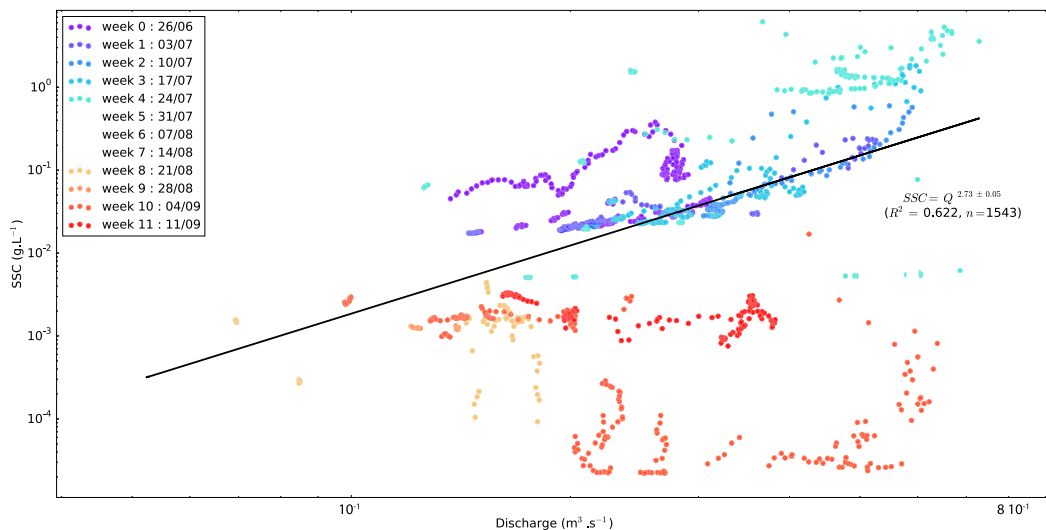
Figure A1. Suspended sediment concentration and discharge upstream and downstream from Bossons proglacial alluvial area during the rain events of 2013 meltseason. Data are grouped by weeks from the start (purple) to the end of the melt season (red). Data are dispersed and a given discharge induces a concentration response across multiple order of magnitude.

Figure A2. Evolution of flux ratio α (entering flux/exiting flux) (blue) and discharge (red). (a–c) during dry periods; (b–d) during precipitation periods; (a,b) At the season scale; (c,d) At the daily scale. Note the logarithmic scale.

Table A1. Statistical fit results for the tested parameter describing the proglacial area dynamics

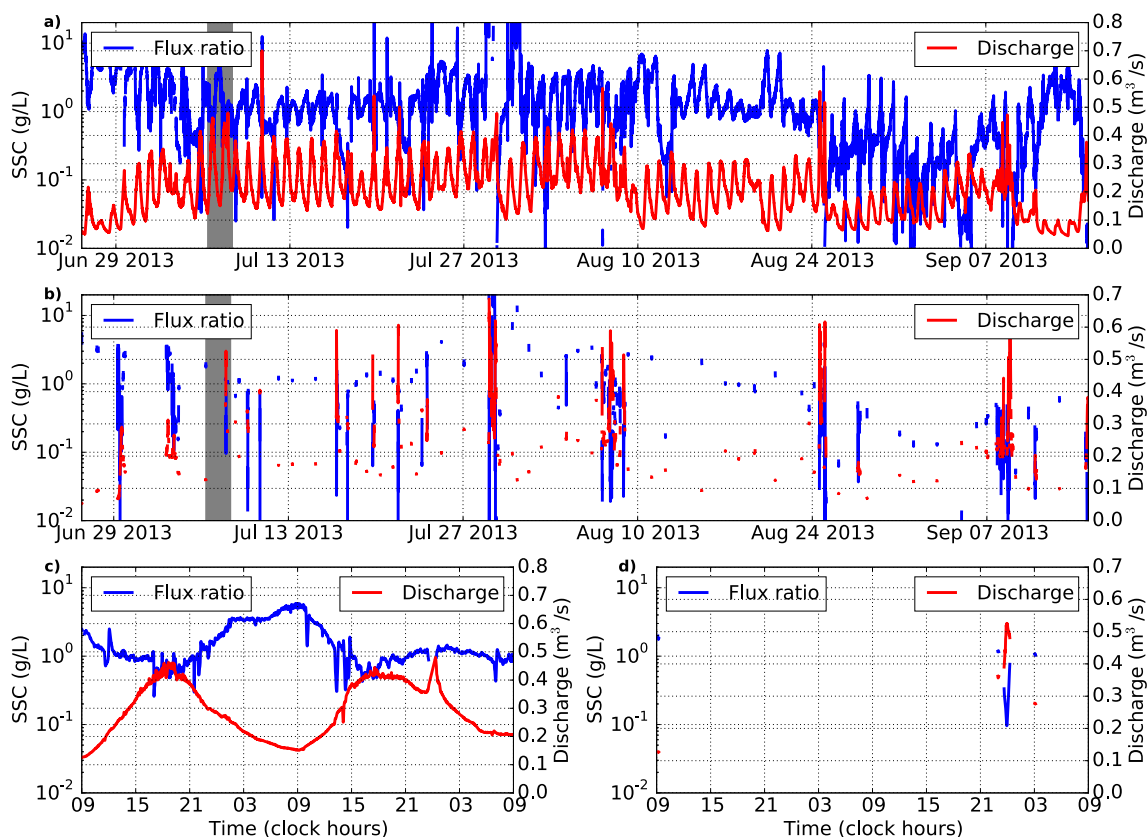| Distributions	$\alpha = F_{\text{in}}/F_{\text{out}}$		α/Q		$\beta = \log_{10}(\alpha)/Q$	
	$-\log \mathscr{L}$	$\sqrt{n}D$	$-\log \mathscr{L}$	$\sqrt{n}D$	$-\log \mathscr{L}$	$\sqrt{n}D$
Cauchy	4170	10.6	8178	10.9	7669	2.14
Chi-squared	3652	12.2	7341	11.5	19,682	39.0
Exponential	5333	16.9	9230	17.7	10,607	17.4
Exponential-Weibull	2780	2.76	**6534**	2.76	7655	3.46
Gamma	6086	26.1	10,163	27.4	7734	4.41
Gumbel left	13,843	21.7	17,822	21.8	7899	5.28
Gumbel right	7288	13.0	11,176	13.1	8306	6.39
Laplace	7126	17.6	11,037	17.8	**7466**	**1.32**
Log-normal	**2845**	3.01	6672	3.38	7697	4.08
Maxwell	9897	17.0	13,754	16.7	8470	10.3
Normal	10,653	16.9	14,522	16.8	7694	4.00
Powerlaw	∞	18.2	∞	12.4	9615	15.4
Power-lognormal	2761	3.50	6566	3.30	7671	3.54
Rayleigh	9747	18.2	13,608,	17.8	8923	12.7
Weibull	3398	14.3	7143	13.2	15,102	33.2

Highlighted in bold are minimum values of negative log-likelihood and the Kolmogorov–Smirnov test values below the critical value.

$-\log \mathscr{L}$: negative log-likelihood (the lower the better); D: Kolmogorov–Smirnov test result (the lower the better); n: sample size; if $\sqrt{n}D$ is greater than a critical value of 1.36, the null hypothesis is rejected.

value of 1.36. We tested 15 candidate distributions: normal, exponential, Weibull, power, exponential-power, exponential-Weibull, Rayleigh, Gumbell, chi-squared, Cauchy, Laplace, log-normal, Maxwell, and power log-normal.

Once a statistical distribution was selected, estimating the entering flux was performed through 10,000 iterations of a Monte-Carlo scheme with four steps. First, for each existing value of the downstream flux, a value of the parameter β was drawn from the parameter distribution. Second, the upstream flux was estimated from the value of the parameter and discharge using (9). Third, the resulting randomly generated flux signal was integrated over time. These three steps were repeated 10,000 times leading to 10,000 values of sediment input entering the proglacial alluvial area. Lastly, the central tendency of the resulting sediment mass was derived by fitting a normal distribution, providing an estimate for the entering sediment flux.

Our extensive statistical analysis confirms the relevance of discharge independent logarithmic ratio of sediment flux (Table A1). A Laplace distribution yields the lowest Kolmogorov–Smirnov value and was selected to estimate β (Table A1). However, examining the resulting β distribution suggests that non-physical values may arise (e.g. an entering flux 10^6 times greater than the exiting flux) and the Laplace distribution was truncated when used to estimate the entering flux.

To further assess the validity of our approach, its output was compared with values measured during the 2013 meltseason (Figure A3). While imperfect, the entering flux calculated from a simple statistical model and from measurements are within one standard deviation from one another. In comparison, the values estimated using a constant ratio and from field measurements are more than one standard deviation apart. In total, estimating the upstream flux with this simple statistical approach lies within the uncertainty range of the measured values and provides a significantly better estimate than simply using a constant ratio, inconsistent with our more recent observations.
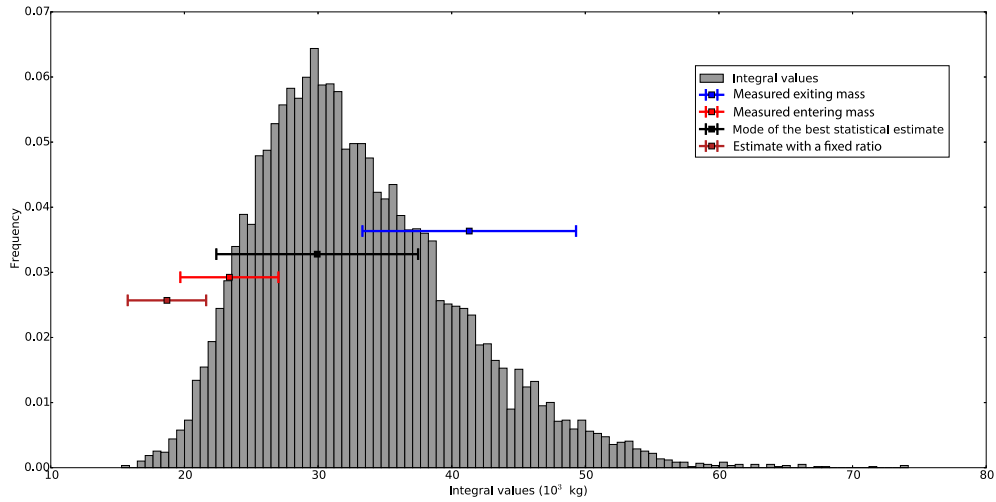
Figure A3. Comparison of methods estimating the mass of sediment entering in the proglacial alluvial area during precipitations of the meltseason. The histogram corresponds to the distribution of the integration results for upstream input. Measured downstream export is displayed in blue; estimated upstream input is displayed in red; the mode of the probability distribution best fitted to the Monte-Carlo simulation outputs is represented in black. Data and estimate of the entering mass are drawn from Guillon et al. [2018].

Table B1. TCN values compiled from Guillon et al. [2015b] and Sarr et al. [2019] to derive supraglacial to subglacial ratio in Bossons glacier catchment

Sample	Position	Latitude (°N)	Longitude (°E)	Altitude (m asl)	$^{10}Be/^{9}Be$	^{10}Be (atoms·g^{-1})	Uncertainty (atoms·g^{-1})	Source
GL-1	PP-right-side	45.88912	6.85819	1817	1.87×10^{-13}	2.38×10^{5}	1.68×10^{4}	[Sarr et al., 2019]
GL-3	PP-right-side	45.88912	6.85819	1817	1.36×10^{-13}	1.52×10^{5}	1.07×10^{4}	[Sarr et al., 2019]
GL-4	PP-right-side	45.88912	6.85819	1817	6.06×10^{-14}	9.50×10^{4}	6.80×10^{3}	[Sarr et al., 2019]
GL-5	PP-left-side	45.88936	6.85579	1765	1.29×10^{-13}	1.45×10^{5}	8.70×10^{3}	[Sarr et al., 2019]
GL-6	PP-left-side	45.88869	6.85539	1810	8.93×10^{-14}	1.41×10^{5}	7.60×10^{3}	[Sarr et al., 2019]
GL-7	PP-centre	45.88957	6.85681	1794	1.38×10^{-13}	1.94×10^{5}	2.54×10^{4}	[Sarr et al., 2019]
GL-18	PG-moraine	45.87954	6.86812	2561	2.88×10^{-14}	3.79×10^{4}	6.20×10^{3}	[Sarr et al., 2019]
GL-19	PG-moraine	45.87954	6.86812	2561	2.17×10^{-14}	3.03×10^{4}	4.50×10^{3}	[Sarr et al., 2019]
GL-20	PG-moraine	45.87954	6.86812	2561	2.32×10^{-14}	4.26×10^{4}	6.50×10^{3}	[Sarr et al., 2019]
GL-21	PG-right-side	45.88028	6.87027	2570	1.34×10^{-14}	1.97×10^{4}	2.40×10^{3}	[Sarr et al., 2019]
Boss supra	PP-left-side	45.88898	6.85865	1795	2.08×10^{-14}	2.72×10^{4}	2.40×10^{3}	[Guillon et al., 2015b]
BOS2A	Bossons subglacial stream	45.89220	6.85244	1443	1.23×10^{-14}	1.52×10^{4}	2.40×10^{3}	[Guillon et al., 2015b]
BOS2B	Bossons subglacial stream	45.89220	6.85279	1441	1.16×10^{-14}	1.10×10^{4}	2.82×10^{3}	[Guillon et al., 2015b]
BOS8	Bossons stream datalogger	45.89940	6.84892	1240	1.6×10^{-14}	1.65×10^{4}	2.69×10^{3}	[Guillon et al., 2015b]
BOS11	Crosette sand	45.89190	6.86003	1760	2.4×10^{-15}	2.12×10^{3}	6.11×10^{2}	[Guillon et al., 2015b]
Boss sous	Crosette subglacial stream	45.89140	6.85917	1760	3.31×10^{-15}	2.53×10^{3}	8.77×10^{2}	[Guillon et al., 2015b]

Appendix B. Cosmogenic nuclides content measurements

See Table B1.

Appendix C. Detailed hydro-sedimentary data
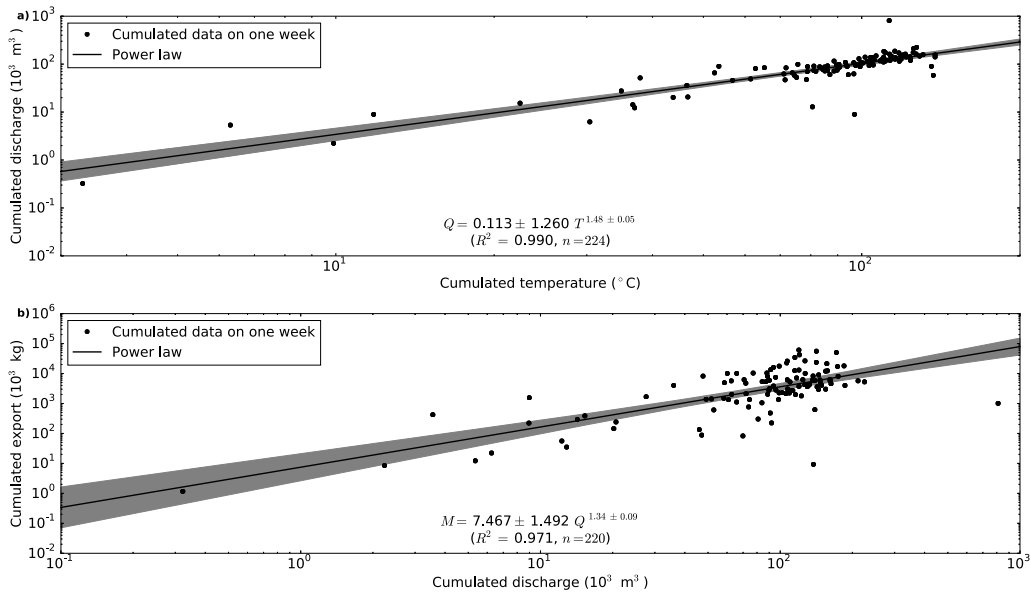
See Tables C1 and C2 and Figure C1.

Figure C1. Relationship between temperature, volume of meltwater and sediment export. (a) Relationship between temperature T and cumulative meltwater discharge Q, integrated over one week periods; (b) relationship between cumulative meltwater discharge Q and sediment export M, integrated over one week periods. (a–b) The gray area represents the boundary for a 99% confidence interval. While the power laws are statistically significant, the relationship between meltwater volume and sediment export (b) exhibits a dispersion over three orders of magnitude.

Table C1. Integration of suspended sediment flux (silts only) at Bossons downstream and Crosette stations

| Stream | Year | Before melt season (10^3 kg) | Melt season | | | After melt season (10^3 kg) |
			During precipitations (10^3 kg)	During dry periods (10^3 kg)	Total (10^3 kg)	
Bossons	2009	n/a	71.6 ± 11.4	111.6 ± 17.75	183.2 ± 29.15	n/a
	2010	n/a	536.5 ± 83.45	162.1 ± 25.08	698.7 ± 108.5	n/a
	2011	n/a	15.9 ± 2.47	56.2 ± 16.2	72.0 ± 18.6	5.3 ± 0.87
	2012	4.93 ± 1.67	32.9 ± 4.93	270.24 ± 45.23	303.1 ± 50.16	n/a
	2013	n/a	63.6 ± 9.4	87.54 ± 20.21	151.18 ± 29.63	10.0 ± 5.04
	2014	n/a	80.1 ± 12.2	149.8 ± 31.34	230.8 ± 43.52	n/a
	2015	18.0 ± 1.88	184.2 ± 25.45	604.2 ± 85.02	788.4 ± 110.5	n/a
	2016	11.1 ± 1.32	n/a	n/a	1299.8 ± 188.4	0.58 ± 0.06
Crosette	2013	n/a	n/a	n/a	305.1 ± 113.9	n/a
	2014	n/a	n/a	n/a	406.8 ± 107.3	n/a
	2016	n/a	n/a	n/a	42.2 ± 7.87	n/a

"n/a" stands for not available.

Table C2. Input during melt season precipitation, total input from upstream sources and total export from the proglacial alluvial area

	Upstream input during meltseason precipitations (10^3 kg)	Total input from upstream sources (glacial input) (10^3 kg)	Total input from valley sandur (10^3 kg)
2009	20.9 ± 73.6	132.5 ± 91.31	50.71 ± 84.96
2010	114.0 ± 50.77	276.1 ± 75.84	422.5 ± 134.2
2011	7.92 ± 3.03	64.1 ± 19.2	13.3 ± 6.37
2012	22.0 ± 6.26	292.2 ± 51.49	15.8 ± 12.86
2013	46.52 ± 9.65	134.1 ± 29.86	27.16 ± 24.1
2014	51.9 ± 6.61	201.7 ± 37.95	29.10 ± 18.8
2015	n/a	n/a	n/a
2016	n/a	n/a	n/a

References

Allen, P. (2005). Striking a chord. *Nature*, 434(7036), 961–961.

Anderson, S. P., Walder, J. S., Anderson, R. S., Kraal, E. R., Cunico, M., Fountain, A. G., and Trabant, D. C. (2003). Integrated hydrologic and hydrochemical observations of Hidden Creek Lake jökulhlaups, Kennicott Glacier, Alaska. *J. Geophys. Res.: Earth Surf.*, 108(F1), article no. 6003.

Avian, M., Kellerer-Pirklbauer, A., and Lieb, G. (2018). Geomorphic consequences of rapid deglaciation at Pasterze Glacier, Hohe Tauern Range, Austria, between 2010 and 2013 based on repeated terrestrial laser scanning data. *Geomorphology*, 310, 1–14.

Baëff, B. (1891). *Les eaux de l'Arve: recherches de géologie expérimentale sur l'érosion et le transport dans les rivières torrentielles ayant des affluents glaciaires*. PhD thesis, University of Geneva.

Ballantyne, C. (2002a). A general model of paraglacial landscape response. *Holocene*, 12(3), 371–376.

Ballantyne, C. K. (2002b). Paraglacial Geomorphology. *Quat. Sci. Rev.*, 21, 1935–2017.

Bartholomaus, T. C., Anderson, R. S., and Anderson, S. P. (2008). Response of glacier basal motion to transient water storage. *Nat. Geosci.*, 1(1), 33–37.

Beaud, F., Flowers, G. E., and Venditti, J. G. (2018). Modeling sediment transport in ice-walled subglacial channels and its implications for esker formation and proglacial sediment yields. *J. Geophys. Res.: Earth Surf.*, 123(12), 3206–3227.

Berthet, J. (2016). *L'évolution géomorphologique des systèmes torrentiels proglaciaires de la vallée de Chamonix-Mont-Blanc, une approche du couplage sédimentaire de la fin du Petit Age Glaciaire au désenglacement récent*. PhD thesis, Université Grenoble Alpes, Grenoble.

Berthier, E., Vadon, H., Baratoux, D., Arnaud, Y., Vincent, C., Feigl, K., Rémy, F., and Legrésy, B. (2005). Surface motion of mountain glaciers derived from satellite optical imagery. *Remote Sens. Environ.*, 95(1), 14–28.

Boissier, R. (1916). *Le charriage des alluvions en suspension dans l'eau de l'Arve*. Bureau des archives, Pierrefitte-sur-Seine.

Bourriquen, M., Mercier, D., Baltzer, A., Fournier, J., Costa, S., and Roussel, E. (2018). Paraglacial coasts responses to glacier retreat and associated shifts in river floodplains over decadal timescales (1966–2016), Kongsfjorden, Svalbard. *Land Degrad. Dev.*, 29(11), 4173–4185.

Canadell, M. B., Escoffier, N., Ulseth, A. J., Lane, S. N., and Battin, T. J. (2019). Alpine glacier shrinkage drives shift in dissolved organic carbon export from quasi-chemostasis to transport-limitation. *Geophys. Res. Lett.*, 46(15), 8872–8881.

Church, M. and Ryder, J. M. (1972). Paraglacial sedimentation: a consideration of fluvial processes conditioned by glaciation. *Geol. Soc. Am. Bull.*, 83, 3059–3072.

Cook, S. J., Swift, D. A., Kirkbride, M. P., Knight, P. G., and Waller, R. I. (2020). The empirical basis for modelling glacial erosion rates. *Nat. Commun.*, 11(1), article no. 759.

Cossart, É. and Fressard, M. (2017). Assessment of structural sediment connectivity within catch-

ments: insights from graph theory. *Earth Surf. Dyn.*, 5(2), 253–268.

Curry, A., Cleasby, V., and Zukowskyj, P. (2006). Paraglacial response of steep, sediment-mantled slopes to post-"Little Ice Age" glacier recession in the central Swiss Alps. *J. Quat. Sci.*, 21, 211–225.

Delaney, I. and Adhikari, S. (2020). Increased subglacial sediment discharge in a warming climate: consideration of ice dynamics, glacial erosion and fluvial sediment transport. *Geophys. Res. Lett.*, 47(7), article no. e2019GL085672.

Ehrbar, D., Schmocker, L., Doering, M., Cortesi, M., Bourban, G., Boes, R., and Vetsch, D. (2018). Continuous seasonal and large-scale periglacial reservoir sedimentation. *Sustainability*, 10(9), article no. 3265.

Eichel, J., Draebing, D., and Meyer, N. (2018). From active to stable: Paraglacial transition of alpine lateral moraine slopes. *Land Degrad. Dev.*, 29(11), 4158–4172.

Fallourd, R., Harant, O., Trouve, E., Nicolas, J.-M., Gay, M., Walpersdorf, A., Mugnier, J.-L., Serafini, J., Rosu, D., Bombrun, L., Vasile, G., Cotte, N., Vernier, F., Tupin, F., Moreau, L., and Bolon, P. (2011). Monitoring temperate glacier displacement by multitemporal TerraSAR-X images and continuous GPS measurements. *IEEE J. Sel. Top. Appl. Earth Obs. Remote Sens.*, 4(2), 372–386.

Fountain, A. G. and Walder, J. S. (1998). Water flow through temperate glaciers. *Rev. Geophys.*, 36(3), 299–328.

Godard, V., Tucker, G. E., Fisher, G. B., Burbank, D. W., and Bookhagen, B. (2013). Frequency-dependent landscape response to climatic forcing. *Geophys. Res. Lett.*, 40(5), 859–863.

Godon, C., Guillon, H., Buoncristiani, J.-F., and Mugnier, J.-L. (2014). Grain size distributions of the Bossons glacier (France). PANGEAE: Data Publisher for Earth & Environmental Science.

Godon, C., Mugnier, J., Fallourd, R., Paquette, J., Pohl, A., and Buoncristiani, J. (2013). The Bossons glacier protects Europe's summit from erosion. *Earth Planet. Sci. Lett.*, 375, 135–147.

Guillon, H. (2016). *Origine et transport des sédiments dans un bassin versant alpin englacé (Glacier des Bossons, France) : Une quantification couplant mesures hydro-sédimentaires haute-résolution, suivi radio-fréquence de galets, teneur en nucléides cosmogéniques et méthodes proba-bilistes.* PhD thesis, Université Grenoble Alpes, Grenoble.

Guillon, H., Godon, C., Buoncristiani, J.-F., and Mugnier, J.-L. (2015a). Hydro-sedimentary parameters measurements within the proglacial area of the Bossons glacier (Mont-Blanc massif, France). PANGEAE: Data Publisher for Earth & Environmental Science.

Guillon, H., Mugnier, J.-L., and Buoncristiani, J.-F. (2018). Proglacial sediment dynamics from daily to seasonal scales in a glaciated Alpine catchment (Bossons glacier, Mont Blanc massif, France). *Earth Surf. Proc. Landf.*, 43(7), 1478–1495.

Guillon, H., Mugnier, J.-L., Buoncristiani, J.-F., Carcaillet, J., Godon, C., Prud'Homme, C., Van der Beek, P., and Vassallo, R. (2015b). Improved discrimination of subglacial and periglacial erosion using 10Be concentration measurements in subglacial and supraglacial sediment load of the Bossons glacier (Mont Blanc massif, France). *Earth Surf. Proc. Landf.*, 40(9), 1202–1215.

Guillon, H., Mugnier, J.-L., Godon, C., Buoncristiani, J.-F., Goutaland, D., Winiarsky, T., and Bièvre, G. (2015c). Sediment volume variations inferred from DGPS measurements within Bossons glacier proglacial area (Mont-Blanc massif, France). PANGEAE: Data Publisher for Earth & Environmental Science.

Hallet, B. (1979). A theoretical model of glacial abrasion. *J. Glaciol.*, 23(89), 39–50.

Hallet, B. (1981). Glacial abrasion and sliding: their dependence on the debris concentration in basal ice. *Annal. Glaciol.*, 2, 23–28.

Herman, F., Beyssac, O., Brughelli, M., Lane, S. N., Leprince, S., Adatte, T., Lin, J. Y. Y., Avouac, J.-P., and Cox, S. C. (2015). Erosion by an Alpine glacier. *Science*, 350(6257), 193–195.

Hinderer, M., Kastowski, M., Kamelger, A., Bartolini, C., and Schlunegger, F. (2013). River loads and modern denudation of the Alps—A review. *Earth-Sci. Rev.*, 118, 11–44.

Huss, M. and Farinotti, D. (2012). Distributed ice thickness and volume of all glaciers around the globe. *J. Geophys. Res.*, 117(F4), article no. F04010.

Iken, A. and Bindschadler, R. A. (1986). Combined measurements of subglacial water pressure and surface velocity of findelengletscher, switzerland: conclusions about drainage system and sliding mechanism. *J. Glaciol.*, 32(110), 101–119.

Iverson, N. R. (2012). A theory of glacial quarrying for landscape evolution models. *Geology*, 40, 679–682.

Jaeger, J. M. and Koppes, M. N. (2016). The role of the cryosphere in source-to-sink systems. *Earth-Sci. Rev.*, 153, 43–76.

Kellerer-Pirklbauer, A., Proske, H., and Strasser, V. (2010). Paraglacial slope adjustment since the end of the Last Glacial Maximum and its long-lasting effects on secondary mass wasting processes: Hauser Kaibling, Austria. *Geomorphology*, 120, 65–76.

Kirkbride, M. P. and Deline, P. (2018). Spatial heterogeneity in the paraglacial response to post-Little Ice Age deglaciation of four headwater cirques in the Western Alps. *Land Degrad. Dev.*, 29(9), 3127–3140.

Klaar, M. J., Kidd, C., Malone, E., Bartlett, R., Pinay, G., Chapin, F. S., and Milner, A. (2014). Vegetation succession in deglaciated landscapes: implications for sediment and landscape stability. *Earth Surf. Proc. Landf.*, 40(8), 1088–1100.

Knight, J. and Harrison, S. (2014). Mountain Glacial and paraglacial environments under global climate change: lessons from the past, future directions and policy implications. *Geogr. Ann.: Ser. A, Phys. Geogr.*, 96(3), 245–264.

Knight, J. and Harrison, S. (2018). Transience in cascading paraglacial systems. *Land Degrad. Dev.*, 29(6), 1991–2001.

Koppes, M., Hallet, B., Rignot, E., Mouginot, J., Wellner, J. S., and Boldt, K. (2015). Observed latitudinal variations in erosion as a function of glacier dynamics. *Nature*, 526(7571), 100–103.

Kovanen, D. and Slaymaker, O. (2015). The paraglacial geomorphology of the Fraser Lowland, southwest British Columbia and northwest Washington. *Geomorphology*, 232, 78–93.

Lane, S. N., Bakker, M., Gabbud, C., Micheletti, N., and Saugy, J.-N. (2017). Sediment export, transient landscape response and catchment-scale connectivity following rapid climate warming and Alpine glacier recession. *Geomorphology*, 277, 210–227.

Larsen, D. J., Finkenbinder, M. S., Abbott, M. B., and Ofstun, A. R. (2016). Deglaciation and post-glacial environmental changes in the Teton Mountain Range recorded at Jenny Lake, Grand Teton National Park, WY. *Quat. Sci. Rev.*, 138, 62–75.

Le Meur, E. and Vincent, C. (2006). Monitoring of the Taconnaz ice fall (French Alps) using measurements of mass balance, surface velocities and ice cliff position. *Cold Reg. Sci. Technol.*, 46(1), 1–11.

Leggat, M. S., Owens, P. N., Stott, T. A., Forrester, B. J., Déry, S. J., and Menounos, B. (2015). Hydro-meteorological drivers and sources of suspended sediment flux in the pro-glacial zone of the retreating Castle Creek Glacier, Cariboo Mountains, British Columbia, Canada. *Earth Surf. Proc. Landf.*, 40(11), 1542–1559.

Mackay, J. D., Barrand, N. E., Hannah, D. M., Krause, S., Jackson, C. R., Everest, J., Aðalgeirsdóttir, G., and Black, A. R. (2019). Future evolution and uncertainty of river flow regime change in a deglaciating river basin. *Hydrol. Earth Syst. Sci. Discuss.*, 23(4), 1833–1865.

Magnin, F., Haeberli, W., Linsbauer, A., Deline, P., and Ravanel, L. (2020). Estimating glacier-bed overdeepenings as possible sites of future lakes in the de-glaciating Mont Blanc massif (Western European Alps). *Geomorphology*, 350, article no. 106913.

Micheletti, N., Lambiel, C., and Lane, S. N. (2015). Investigating decadal-scale geomorphic dynamics in an alpine mountain setting. *J. Geophys. Res. Earth Surf.*, 120(10), 2155–2175.

Moon, S., Shelef, E., and Hilley, G. E. (2015). Recent topographic evolution and erosion of the deglaciated Washington Cascades inferred from a stochastic landscape evolution model. *J. Geophys. Res.: Earth Surf.*, 120(5), 856–876.

Morin, G. P., Lavé, J., France-Lanord, C., Rigaudier, T., Gajurel, A. P., and Sinha, R. (2018). Annual sediment transport dynamics in the narayani basin, Central Nepal: assessing the impacts of erosion processes in the annual sediment budget. *J. Geophys. Res.: Earth Surf.*, 123(10), 2341–2376.

Nanni, U., Gimbert, F., Vincent, C., Gräff, D., Walter, F., Piard, L., and Moreau, L. (2020). Quantification of seasonal and diurnal dynamics of subglacial channels using seismic observations on an Alpine glacier. *Cryosphere Discuss.*, 14(5), 1475–1496.

O'Briain, R. (2019). Climate change and european rivers: An eco-hydromorphological perspective. *Ecohydrology*, 12(5), article no. e2099.

Owen, L. A. and Sharma, M. C. (1998). Rates and magnitudes of paraglacial fan formation in the Garhwal Himalaya: implications for landscape evolution. *Geomorphology*, 26, 171–184.

Rada, C. and Schoof, C. (2018). Channelized, dis-

tributed, and disconnected: subglacial drainage under a valley glacier in the Yukon. *Cryosphere*, 12(8), 2609–2636.

Rainato, R., Mao, L., García-Rama, A., Picco, L., Cesca, M., Vianello, A., Preciso, E., Scussel, G., and Lenzi, M. (2016). Three decades of monitoring in the Rio Cordon instrumented basin: Sediment budget and temporal trend of sediment yield. *Geomorphology*, 291, 45–56.

Ravazzi, C., Badino, F., Marsetti, D., Patera, G., and Reimer, P. J. (2012). Glacial to paraglacial history and forest recovery in the Oglio glacier system (Italian Alps) between 26 and 15 ka cal BP. *Quat. Sci. Rev.*, 58, 146–161.

Riihimaki, C. A. (2005). Sediment evacuation and glacial erosion rates at a small alpine glacier. *J. Geophys. Res.*, 110(F3), article no. F03003.

Rothlisberger, H. and Lang, H. (1987). *Glacial Hydrology*. Wiley, Hoboken, NJ. Ch. 10.

Sarr, A.-C., Mugnier, J.-L., Abrahami, R., Carcaillet, J., and Ravanel, L. (2019). Sidewall erosion: Insights from in situ-produced 10Be concentrations measured on supraglacial clasts (Mont Blanc massif, France). *Earth Surf. Proc. Landf.*, 44(10), 1930–1944.

Savi, S., Norton, K. P., Picotti, V., Akcar, N., Delunel, R., Brardinoni, F., Kubik, P., and Schlunegger, F. (2014). Quantifying sediment supply at the end of the last glaciation: Dynamic reconstruction of an alpine debris-flow fan. *Geol. Soc. Am. Bull.*, 126(5–6), 773–790.

Staines, K. E. H., Carrivick, J. L., Tweed, F. S., Evans, A. J., Russell, A. J., Jóhannesson, T., and Roberts, M. (2014). A multi-dimensional analysis of pro-glacial landscape change at Sólheimajökull, southern Iceland. *Earth Surf. Proc. Landf.*, 40(6), 809–822.

Swift, D. A., Nienow, P. W., Spedding, N., and Hoey, T. B. (2002). Geomorphic implications of subglacial drainage configuration: rates of basal sediment evacuation controlled by seasonal drainage system evolution. *Sediment. Geol.*, 149(1–3), 5–19.

Ugelvig, S. V., Egholm, D. L., Anderson, R. S., and Iverson, N. R. (2018). Glacial erosion driven by variations in meltwater drainage. *J. Geophys. Res.: Earth Surf.*, 123(11), 2863–2877.

Vincent, C., Fischer, A., Mayer, C., Bauder, A., Galos, S. P., Funk, M., Thibert, E., Six, D., Braun, L., and Huss, M. (2017). Common climatic signal from glaciers in the European Alps over the last 50 years. *Geophys. Res. Lett.*, 44(3), 1376–1383.

Vincent, C., Le Meur, E., Six, D., Funk, M., Hoelzle, M., and Preunkert, S. (2007). Very high-elevation Mont Blanc glaciated areas not affected by the 20th century climate change. *J. Geophys. Res.*, 112, article no. D09120.

Zekollari, H., Huss, M., and Farinotti, D. (2018). Modelling the future evolution of glaciers in the European Alps under the EURO-CORDEX RCM ensemble. *Cryosphere Discuss.*, 13(4), 1125–1146.